IOPscience iopscience.iop.org

Home Search Collections Journals About Contact us My IOPscience

Orbital photogalvanic effects in quantum-confined structures

This article has been downloaded from IOPscience. Please scroll down to see the full text article.

2010 J. Phys.: Condens. Matter 22 355307

(http://iopscience.iop.org/0953-8984/22/35/355307)

View the table of contents for this issue, or go to the journal homepage for more

Download details:
IP Address: 132.199.98.18
The article was downloaded on 30/08/2010 at 07:20

Please note that terms and conditions apply.

IOP PUBLISHING JOURNAL OF PHYSICS: CONDENSED MATTER
J. Phys.: Condens. Matter **22** (2010) 355307 (9pp) doi:10.1088/0953-8984/22/35/355307

Orbital photogalvanic effects in quantum-confined structures

J Karch[1], S A Tarasenko[2], P Olbrich[1], T Schönberger[1], C Reitmaier[1], D Plohmann[1], Z D Kvon[3] and S D Ganichev[1]

[1] Terahertz Center, University of Regensburg, 93040 Regensburg, Germany
[2] Ioffe Physical-Technical Institute, Russian Academy of Sciences, 194021 St Petersburg, Russia
[3] Institute of Semiconductor Physics, Russian Academy of Sciences, 630090 Novosibirsk, Russia

E-mail: sergey.ganichev@physik.uni-regensburg.de

Received 20 April 2010, in final form 28 July 2010
Published 18 August 2010
Online at stacks.iop.org/JPhysCM/22/355307

Abstract
We report on the circular and linear photogalvanic effects caused by free-carrier absorption of terahertz radiation in electron channels on (001)-oriented and miscut silicon surfaces. The photocurrent behaviour upon variation of the radiation polarization state, wavelength, gate voltage, and temperature is studied. We present the microscopic and phenomenological theory of the photogalvanic effects, which describes well the experimental results. In particular, it is demonstrated that the circular (photon-helicity sensitive) photocurrent in silicon-based structures is of pure orbital nature originating from the quantum interference of different pathways contributing to the absorption of monochromatic radiation.

1. Introduction

The photogalvanic effects, linear (LPGE) and circular (CPGE), representing the generation of a directed electric current due to the asymmetry of photoexcitation or relaxation processes attract growing attention. They can occur in media of sufficiently low spatial symmetry only and are known to be an efficient tool to study nonequilibrium processes in semiconductor structures yielding information on their symmetry, details of the band spin splitting, momentum, energy and spin relaxation times, etc (for a review see, e.g., [1–4]). Moreover, the photogalvanic effects are applied for the detection of the polarization state of infrared and terahertz (THz) laser radiation [5]. The low spatial symmetry required for the photogalvanic effects is naturally realized in non-centrosymmetric bulk semiconductors and low-dimensional structures based on them. However, it has been shown that both the LPGE and the CPGE can occur in two-dimensional structures made of centrosymmetric crystals, e.g., silicon, due to the structure inversion asymmetry [6–8]. The LPGE in silicon metal–oxide–semiconductor field-effect-transistors (Si-MOSFETs) was observed almost twenty years ago [9], but the first experiments on the CPGE, a photocurrent reversing its direction upon switching the sign of circular polarization, have been reported only most recently [10]. Besides the fundamental interest to photogalvanics, a renaissance in the study of photoelectrical phenomena in MOSFETs is additionally stimulated by the prospect of their application for the emission and detection of THz radiation [11]. Preliminary results on the circular photogalvanic effect in MOSFETs have been reported in [10]. These experiments were done on MOSFETs fabricated on miscut silicon surfaces and provided the first proof that the photon-helicity sensitive photocurrent can be not only of spin-dependent origin, as commonly considered [12–15], but also be due to pure orbital effects. While the fact of the existence of orbital mechanisms of the CPGE has been demonstrated, several questions remain open. First of all, photogalvanic effects in Si-MOSFETs have so far been observed in miscut structures only. An essential ingredient in the current formation for this particular case is the peculiarity of the silicon band structure, namely, the in-plane anisotropy of the electron energy spectrum in two-dimensional valleys. It is, therefore, not clear whether the polarization dependent photocurrents can be substantial as well in two-dimensional systems with a simple parabolic dispersion in the channel plane. To solve the problem, we study here the photogalvanic effects in MOSFETs on precisely oriented (001) silicon surfaces. The experiments demonstrate that both circular and linear photogalvanic currents can be

 © 2010 IOP Publishing Ltd Printed in the UK & the USA

generated in (001)-oriented structures being of the same order of magnitude as compared to those in MOSFETs on miscut surfaces. To describe the experimental observation we develop a phenomenological theory of the photogalvanic effects and present the detailed microscopic theory of the CPGE introduced in [8, 10]. Now, the theory includes the CPGE in precisely oriented (001) structures and, for miscut structures, the description is not any more limited to the case of small inclination angles as it was in [10]. The second challenge is the description of the photocurrent spectral behaviour. The reversal of the current direction upon variation of the gate voltage, previously observed in miscut structures at low temperature only and attributed to the point of the intersubband resonance condition [10], is studied now in detail as a function of temperature, excitation wavelength, and inclination angle for miscut samples. The obtained results, together with literature data, confirm this conclusion. The same result comes from the developed theory for both types of structures which, for MOSFETs on (001)-oriented surfaces, now includes the spectral dependence of the circular photocurrent in the intersubband resonance vicinity, which was out of the scope in [8]. We also give a comprehensive study of the linear photogalvanic effect at direct and, previously not reported, indirect optical transitions. The LPGE current is insensitive to the photon-helicity sign, it can be induced by linearly polarized light and also be treated as a quantum ratchet effect [16].

This paper is organized as follows. In section 2, we present the phenomenological theory of the LPGE and CPGE in two-dimensional channels on (001) precisely oriented as well as miscut silicon surfaces. In section 3, a short overview of the experimental technique used is given. The experimental results are summarized in section 4 and compared with the phenomenological theory. In section 5, we present a microscopic theory of the CPGE caused by the quantum interference of optical transitions for both types of structures. Finally, in section 6, we discuss the experimental data in view of the theoretical background.

2. Phenomenological theory

Phenomenologically, the density of the photocurrent $\boldsymbol{j}$ emerging in an unbiased structure within the linear regime in the radiation intensity is given by [7]

$$j_\alpha = \sum_{\beta\gamma} \chi_{\alpha\beta\gamma} \frac{E_\beta E_\gamma^* + E_\gamma E_\beta^*}{2} + \sum_\beta \mu_{\alpha\beta} \mathrm{i}[\boldsymbol{E} \times \boldsymbol{E}^*]_\beta, \quad (1)$$

where $\boldsymbol{\chi}$ is a third-rank tensor that is symmetric in the last two indices, $\boldsymbol{\mu}$ is a second-rank pseudotensor, $\boldsymbol{E} = |\boldsymbol{E}|\boldsymbol{e}$ is the electric field of the radiation in the channel, $\boldsymbol{e}$ is the (complex) unit vector of the light polarization, α, β and γ are the Cartesian coordinates, and the photon wavevector is neglected in equation (1). The tensor $\boldsymbol{\chi}$ describes the photocurrent which can be induced by linearly polarized or unpolarized radiation. By contrast, $\boldsymbol{\mu}$ stands for the photocurrent which is sensitive to the radiation helicity and reverses its direction upon switching the sign of the circular polarization, because $\mathrm{i}[\boldsymbol{E} \times \boldsymbol{E}^*] = |\boldsymbol{E}|^2 P_{\mathrm{circ}} \hat{\boldsymbol{e}}$ with the degree of circular polarization P_{circ} and the unit vector $\hat{\boldsymbol{e}}$ pointing in the light propagation direction. Non-zero components of the tensors $\boldsymbol{\chi}$ and $\boldsymbol{\mu}$ can be obtained by analysing the spatial symmetry of structures.

We consider the linear and circular photogalvanic effects for the two point-group symmetries $C_{\infty v}$ and C_s, which are relevant to electron channels on precisely (001) oriented and miscut silicon surfaces, respectively. Two-dimensional channels on a (001) surface can be effectively described by the axial point-group $C_{\infty v}$, which takes into account the structure inversion asymmetry of the channel. In such structures, the photocurrent can be excited only at oblique incidence of radiation, and its components are given by the phenomenological equations

$$\begin{aligned} j_x &= L(E_x E_z^* + E_z E_x^*) + C\mathrm{i}[\boldsymbol{E} \times \boldsymbol{E}^*]_y, \\ j_y &= L(E_y E_z^* + E_z E_y^*) - C\mathrm{i}[\boldsymbol{E} \times \boldsymbol{E}^*]_x, \end{aligned} \quad (2)$$

where the first and second terms on the right-hand side of equations (2) stand for the linear and circular photogalvanic effects, respectively, x and y are the in-plane axes, and $z \parallel [001]$ is the channel normal.

The channels fabricated on miscut surfaces exhibit the lower point-group symmetry C_s due to the deviation of the channel plane from (001) together with the asymmetry of the confinement potential [6, 7]. In structures of the C_s point group, both linear and circular photogalvanic effects are allowed even at normal incidence of radiation [14]. In this particular geometry, the photocurrent components are phenomenologically described by

$$\begin{aligned} j_{x'} &= L_1'(E_{x'} E_{y'}^* + E_{y'} E_{x'}^*) + C'\mathrm{i}[\boldsymbol{E} \times \boldsymbol{E}^*]_{z'}, \\ j_{y'} &= L_2' + L_3'(|E_{x'}|^2 - |E_{y'}|^2). \end{aligned} \quad (3)$$

Here, we assume that the channel plane $(x'y')$ is tilted from the plane (001) around the axis $x' \parallel [1\bar{1}0]$, and z' is the channel normal. In contrast to (001)-oriented MOSFETs, the photocurrent in structures on miscut surfaces can be induced even by unpolarized radiation.

3. Samples and experimental techniques

In our experiments, we study photocurrents in MOSFETs fabricated on (001)-oriented and miscut silicon surfaces. On the precisely oriented (001) surface, a transistor along $y \parallel [110]$ with a channel length of 3 mm and a width of 2.8 mm was prepared with a 110 nm thick SiO_2 layer, a semitransparent polycrystalline Si gate and a doping level N_a of the depletion layer of about 3×10^{15} cm^{-3}. In this transistor, the variation of the gate voltage V_g from 1 to 20 V changes the carrier density N_s from about 1.9×10^{11} to 3.8×10^{12} cm^{-2} and the energy spacing ε_{21} between the size-quantized subbands $e1$ and $e2$ from 10 to 35 meV. The peak mobilities μ at room and helium temperature are 700 and 10^4 cm^2 V^{-1} s^{-1}, respectively. Another set of MOSFETs was fabricated on miscut surfaces tilted by an angle of $\vartheta = 9.7°$ or $10.7°$ from the (001) plane around $x' \parallel [1\bar{1}0]$. Two transistors were prepared on each miscut substrate, one oriented along x' and the other along the inclination direction parallel to y'. They have a size of

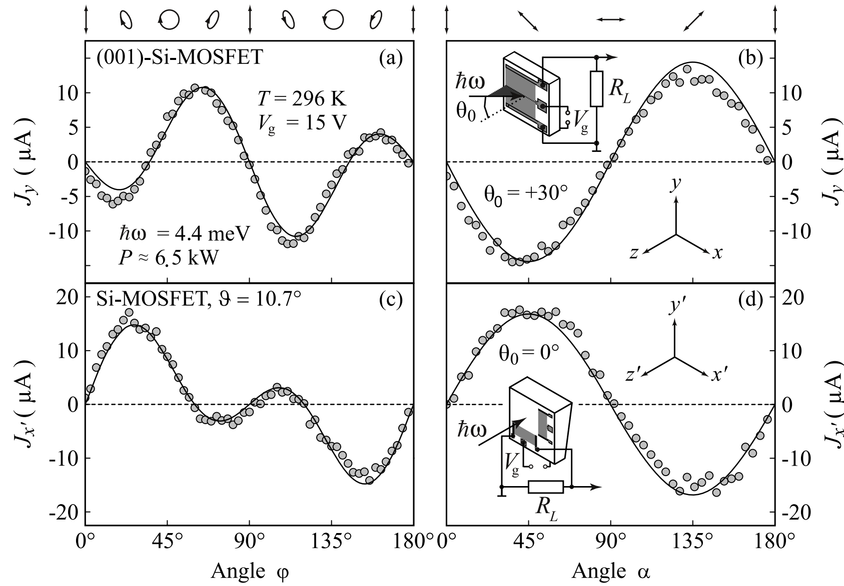

Figure 1. Polarization dependences of the photocurrent measured in transistors on the (001)-oriented surface ((a) and (b)) and on the miscut surface ((c) and (d)). Panels (a) and (c) show the photocurrent as a function of the angle φ, which determines the radiation helicity. Panels (b) and (d) show the photocurrent measured as a function of the azimuth angle α for gate voltage of 15 V. The data are obtained at room temperature applying radiation with the photon energy 4.4 meV, the power ≈6.5 kW, and the diameter of the laser spot of about 2.5 mm. The insets sketch the experimental setups for the different structures: the (001)-MOSFET is illuminated at oblique incidence with the angle $\theta_0 = 30°$ and the miscut sample at normal incidence. The polarization states of the radiation for various angles φ and α are illustrated at the top.

1.2×0.4 mm^2, semitransparent Ti gates of 10 nm thickness and a doping concentration N_a of about 1×10^{13} cm^{-3}. A variation in the gate voltage from 1 to 20 V changes the carrier density N_s from 1.5×10^{11} to 3.0×10^{12} cm^{-2} and the energy spacing ε_{21} from 5 to 28 meV. The peak electron mobilities μ in the channel are about 10^3 and 2×10^4 cm^2 V^{-1} s^{-1} at $T = 296$ and 4.2 K, respectively. The MOSFETs on miscut surfaces have a 140 nm thick SiO_2 layer.

For optical excitation we use the emission of a terahertz molecular gas laser, optically pumped by a transversely excited atmosphere pressure (TEA) CO_2 laser [3]. With NH_3 as active gas, 100 ns pulses of radiation with a peak power $P \approx 30$ kW are obtained at the wavelengths $\lambda = 76$, 90, 148 and 280 μm (corresponding to the photon energies $\hbar\omega = 16.3$, 13.7, 8.4 and 4.4 meV, respectively). The laser beam has an almost Gaussian form which was measured with a pyroelectric camera 'Spiricon'. It was focused by means of parabolic mirror in a typical focal spot diameter of about 1.5 to 2.5 mm. The terahertz radiation causes in Si-MOSFETs indirect (Drude-like) optical transitions or direct resonant intersubband transitions, which can be tuned by the gate voltage. Various polarization states of the radiation are achieved by transmitting the linearly polarized laser beam through $\lambda/2$ or $\lambda/4$ crystal quartz plates. By applying $\lambda/2$ plates the angle α between the plane of linear polarization and the y or y' axis is varied from $\alpha = 0°$ to 180° covering all possible orientations of the electric field vector. By rotating a $\lambda/4$ plate we obtain elliptically and, in particular, circularly polarized light. The polarization states are then described by the angle φ between the initial polarization of the laser light ($\boldsymbol{E} \parallel y$ or y') and the optical axis of the plate. The degree of circular polarization in this setup is given by $P_{\rm circ} = \sin 2\varphi$. The light polarization states for some characteristic angles φ are sketched at the top of figure 1(a). The miscut and (001)-oriented samples are excited at normal and oblique incidence, respectively. In the case of oblique incidence, the angle θ_0 between the light propagation direction and the sample normal is $\pm 30°$. The photocurrents are measured between the source and drain contacts of the unbiased transistors via the voltage drop across a load resistor $R_L = 50\ \Omega$, which was much smaller than the source–drain resistance of our transistors. The experimental geometries are illustrated in the insets of figure 1.

4. Experiments

Irradiating the MOSFET structures with THz radiation we observed photocurrent signals with a temporal shape reproducing that of the laser pulse of about 100 ns duration. Figure 1 shows polarization dependences of the measured currents in the y direction on the (001) precisely oriented surface (figures 1(a) and (b)) and in the transistor along x' on the miscut surface (figures 1(c) and (d)). The data are obtained at oblique and normal incidence of radiation for the (001)-oriented and miscut structures, respectively.

First, we discuss the polarization dependences of the photocurrent in (001)-oriented structures. Figure 1(a) shows the photocurrent $J_y(\varphi)$ measured perpendicular to the light propagation at oblique incidence of radiation in the plane (xz) for the angle $\theta_0 = 30°$. The light polarization states for several angles φ are sketched at the top of figure 1(a). Obviously the signal reverses its sign upon switching the radiation helicity from left- to right-handed circular polarization. This

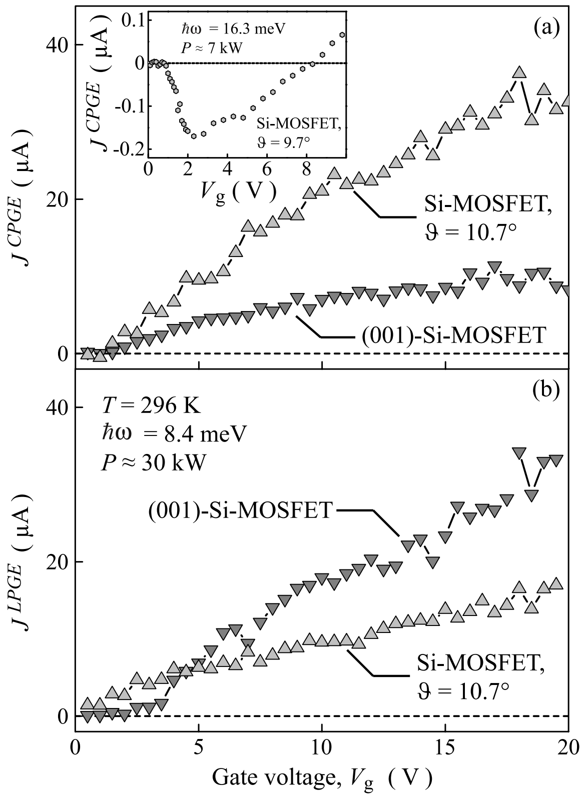

Figure 2. Gate voltage dependences of (a) the circular and (b) the linear photogalvanic currents measured in transistors on the (001)-oriented surface and the miscut surface with $\vartheta = 10.7°$. The data are obtained at room temperature applying radiation at oblique incidence with $\theta_0 = 30°$ for (001)-oriented structures and at normal incidence for miscut transistors. The photocurrents are measured for the photon energy 8.4 meV, the power ≈30 kW, and the diameter of the laser spot of about 2 mm. The inset shows the gate voltage dependence of the circular photocurrent for the photon energy 16.3 meV measured in the miscut MOSFET with inclination angle of 9.7°.

is the characteristic fingerprint of the circular photogalvanic effect [1–4]. In addition, the photocurrent has a contribution independent of the photon helicity. The whole dependence $J_y(\varphi)$ can be well fitted by

$$J(\varphi) = (J_L/2)\sin 4\varphi + J_C \sin 2\varphi \qquad (4)$$

with comparable parameters J_L and J_C. Such a dependence is in full agreement with the phenomenological equation (2) since the polarization dependent terms are reduced to $(E_y E_z^* + E_z E_y^*) = -(E_0^2 t_p t_s/2)\sin\theta \sin 4\varphi$ and $\mathrm{i}[\boldsymbol{E} \times \boldsymbol{E}^*]_x = E_0^2 t_p t_s \sin\theta \sin 2\varphi$ in this experimental geometry. Here, E_0 is the electric field amplitude of the incident light, t_p and t_s are the amplitude transmission coefficients for s- and p-polarized radiation, θ is the angle of refraction related to the incidence angle by $\sin\theta = \sin\theta_0/n_\omega$ with n_ω being the refraction index of the medium. The first and second terms on the right-hand side of equation (4) correspond to the linear and circular photogalvanic effects, respectively, see section 2. Varying the angle of incidence θ_0 from −30° to +30° we observed that both contributions to the photocurrent reverse their signs. Moreover, by changing the plane of incidence from (xz) to (yz), we obtained that the photon-helicity current in the y direction vanishes and only the LPGE contribution remains. All these features correspond to the phenomenological equation (2).

Equation (2) demonstrates that the photocurrent can also be induced by linearly polarized radiation. In this case, the signal should solely be caused by the LPGE, because the CPGE vanishes for linear polarization. The dependence of J_y on the azimuth angle α is given in figure 1(b) and can be well fitted by

$$J(\alpha) = J_L \sin 2\alpha \qquad (5)$$

with the same parameter J_L used in equation (4). This behaviour is also expected from equation (2), because $(E_y E_z^* + E_z E_y^*) = -E_0^2 t_p t_s \sin\theta \sin 2\alpha$.

Now we turn to the transistors made on miscut surfaces. In contrast to (001)-oriented structures, here we observed a photocurrent even at normal incidence of radiation (figures 1(c) and (d)). This difference follows from the symmetry arguments discussed above, see equations (2) and (3). The photon-helicity dependent current is detected only in the transistor along $x' \parallel [1\bar{1}0]$, therefore, we focus below on this particular geometry. The polarization dependences $J_{x'}(\varphi)$ and $J_{x'}(\alpha)$ can also be fitted by equations (4) and (5), respectively, with another set of fitting parameters. They are in accordance with the phenomenological equation (3) since at normal incidence $(E_{x'} E_{y'}^* + E_{y'} E_{x'}^*) = -(1/2)(E_0 t_s)^2 \sin 4\varphi$, $\mathrm{i}[\boldsymbol{E} \times \boldsymbol{E}^*]_{z'} = -(E_0 t_s)^2 \sin 2\varphi$, and $(E_{x'} E_{y'}^* + E_{y'} E_{x'}^*) = -(E_0 t_s)^2 \sin 2\alpha$. However, we emphasize that, in contrast to (001)-oriented structures, the photocurrent direction in miscut samples is determined by the crystallographic axes rather than by the light propagation direction.

The contributions of the circular and linear photogalvanic effects persist for all applied gate voltages from 1 to 20 V, photon energies, and temperatures used in our experiments on both types of MOSFETs. First we discuss the gate voltage dependences of the CPGE (figure 2(a)) and LPGE (figure 2(b)) contributions, i.e., $J_C = [J(\varphi = 45°) - J(\varphi = 135°)]/2$ and $J_L = [J(\alpha = 45°) - J(\alpha = 135°)]/2$, respectively, obtained at room temperature[4]. For the photon energy $\hbar\omega = 8.4$ meV, as well as most other studied wavelengths, the increase in the gate voltage results in a rise of the photocurrent magnitude. Such a behaviour can be attributed to the increase of electron density in the inversion channel and, therefore, the enhancement of the Drude absorption. However, while the LPGE contribution always increases with V_g, the CPGE current at some photon energies exhibits a sign inversion with increasing V_g, as demonstrated for the photon energy $\hbar\omega = 16.3$ meV in the inset in figure 2(a). We note that we cannot attribute the gate voltage corresponding to the sign inversion, V_g^{inv}, to any characteristic energy in the band structure of silicon-based quantum-confined channels.

The most spectacular discrepancy in the CPGE and LPGE behaviour emerges at helium temperature. While the polarization dependences remain the same, the gate voltage dependences become consistently different. In contrast to

[4] We note that for $\varphi = 45°$ and 135° the light is circularly polarized and the LPGE vanishes. For linearly polarized radiation, e.g. for $\alpha = 45°$ and 135°, CPGE is absent.

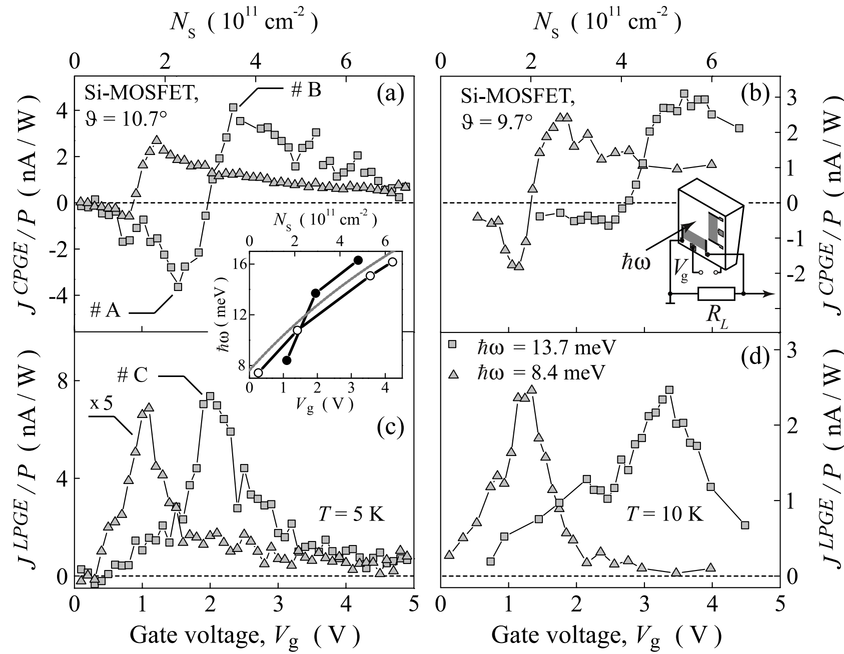

Figure 3. Gate voltage dependences of the circular photogalvanic current ((a) and (b)) and linear photogalvanic current ((c) and (d)) measured in transistors on miscut surfaces with different inclination angles normalized to the laser power. The data are obtained at low temperatures for the photon energies 8.4 and 13.7 meV. The symbols #A, #B and #C denote the gate voltages at which the temperature dependences of figure 4 are measured. The full circles in the inset show the relation between the photon energy and gate voltage of the inversion point of the CPGE. The solid curve and open circles in the inset show the relation between the photon energy and gate voltage corresponding to the intersubband resonance in (001)-oriented MOSFETs calculated numerically [17] and obtained by absorption measurements [18], respectively.

the smooth behaviour observed at room temperature, at helium temperature the LPGE current exhibits a resonance-like response and the CPGE photocurrent shows always a sign inversion. This is shown in figure 3 for two miscut Si-MOSFETs with different angles of inclination $\vartheta = 10.7°$ and $9.7°$. The peak position of the LPGE current, which coincides with the inversion point of the CPGE, depends on the photon energy $\hbar\omega$ and corresponds to $\hbar\omega \approx \varepsilon_{21}$, where ε_{21} is the energy separation of the first two electron subbands. The latter is in accordance with band structure calculations [17] and experiments on far infrared absorption [18] (see inset to figure 3) as well as with our photoconductivity measurements (not shown). The resonance condition is obtained by tuning the energy separation between the first two electron subbands ε_{21} to the photon energy $\hbar\omega$ by changing the gate voltage: the increase in the photon energy shifts the intersubband resonance to larger gate voltages [19]. The discrepancy in the resonance positions, observed in the two miscut samples for a fixed photon energy, is attributed to the difference of their inclination angles.

By increasing the temperature from liquid helium to room temperature the resonant peak of the LPGE and as well as the sign inversion of the CPGE at $\hbar\omega \approx \varepsilon_{21}$ vanish. This is shown in figure 4 for three characteristic gate voltages: all three signals remain almost constant below about 35 K and decrease at higher temperatures. The insets in figures 4(a) and (b) demonstrate that the voltage $V_g^{\rm inv}$ corresponding to the inversion point of the CPGE and the voltage $V_g^{\rm peak}$ of the peak position of the LPGE do not shift with temperature as far as they are detectable. This observation is in agreement with the behaviour of $\varepsilon_{21}(T)$ well known for MOSFETs [19]. At $T > 120$ K, the gate voltage dependences of the current contributions become smooth and similar to those observed at room temperature.

5. Microscopic theory of the CPGE

The microscopic theory of the photogalvanic effects caused by intersubband optical transitions in silicon-based low-dimensional structures was developed in [6]. This theory describes well the resonance behaviour of the linear photogalvanic effect measured at low temperatures. The observation of the photogalvanic effects apart from the intersubband resonance demonstrates that the free-carrier absorption also gives rise to a polarization dependent photocurrent. Below we present the microscopic theory of the CPGE in both (001)-oriented and miscut Si-MOSFETs. As addressed above, the generation of helicity dependent photocurrents in silicon-based structures is of particular interest, because spin-related mechanisms of the CPGE are ineffective due to the vanishingly small constant of spin–orbit coupling in silicon. Therefore, less studied pure orbital mechanisms determine the current formation. We consider this process theoretically following [8] and calculate the photocurrent taking into account the peculiarity of the silicon band structure.

We recall that the electron subbands in Si structures are formed by six valleys X, X', Y, Y', Z, and Z' located at the Δ points of the Brillouin zone of the bulk crystal. The electron dispersion in each valley is anisotropic and described by two

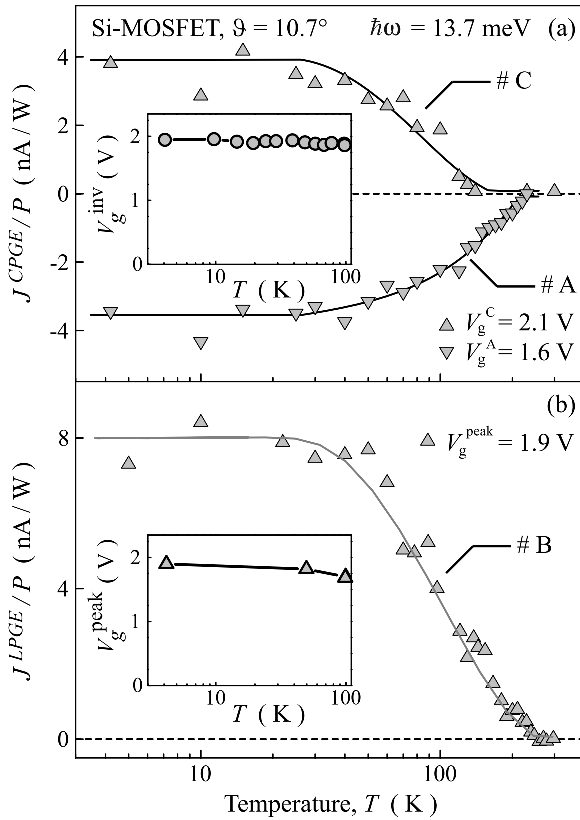

Figure 4. Temperature dependences of (a) the circular and (b) the linear photogalvanic currents measured in the transistor on the miscut surface with $\vartheta = 10.7°$ for $\hbar\omega = 13.7$ meV at characteristic gate voltages indicated by the symbols #A, #B, and #C in figure 3. The insets demonstrate that the gate voltage corresponding to the CPGE sign inversion V_g^{inv} as well as the gate voltage corresponding to the LPGE peak V_g^{peak} are almost independent of the temperature.

different effective masses: longitudinal $m_\parallel$ and transverse $m_\perp$ with respect to the principal axis of the valley. Due to quantum confinement, only two valleys, Z and Z', are occupied at low temperatures and low electron densities in structures grown along $z \parallel [001]$, while the other four valleys are considerably higher in energy. The low-energy valleys are almost equivalent and can be treated independently, because the valley splitting caused by the asymmetry of the confining potential is negligible in comparison to the kinetic energy of electrons and because inter-valley scattering is much weaker than intra-valley processes.

5.1. The CPGE in (001)-oriented structures

The model illustrating the generation of the photocurrent due to free-carrier absorption of circularly polarized radiation is sketched in figure 5. Figure 5(a) shows indirect optical transitions within the subband $e1$ (we assume that only the ground subband $e1$ is populated in the equilibrium). For fulfilling the conditions of energy and momentum conservation, the transitions can only occur if the electron–photon interaction is accompanied by simultaneous electron scattering by phonons or static defects. Such indirect transitions are theoretically treated as second-order virtual processes via intermediate states. The intermediate states can be those within the same quantum subband $e1$ as well as in other conduction or valence subbands. Figures 5(b) and (d) show possible absorption pathways with intermediate states in the subband $e1$ and the excited subband $e2$.

The pathway which is usually considered and which determines the structure absorbance at normal incidence involves intermediate states within the subband $e1$. Such transitions (path I) are shown in figures 5(b) and (c) for the process where the electron–photon interaction is followed by electron scattering (figure 5(b)), and the inverted sequence process (figure 5(c)). The matrix element of such kind of processes has the form

$$M^{(1)}_{\mathbf{k}'\mathbf{k}} = \frac{eA}{c\omega m_\perp} \boldsymbol{e} \cdot (\boldsymbol{k}' - \boldsymbol{k}) V_{11}, \tag{6}$$

where $\boldsymbol{k}$ and $\boldsymbol{k}'$ are the initial and final electron wavevectors, respectively, e is the electron charge, c is the speed of light, A is the amplitude of the vector potential of the electromagnetic wave, which is related to the radiation intensity by $I = A^2\omega^2 n_\omega/(2\pi c)$, and V_{11} is the matrix element of electron scattering within the subband $e1$. We note that, while the matrix element in equation (6) is odd in the wavevector, the absorption probability given by the squared matrix element is even in $(\boldsymbol{k}' - \boldsymbol{k})$. Thus, this type of processes alone does not introduce any asymmetry in the carrier distribution in $\boldsymbol{k}$-space and, consequently, does not yield an electric current.

In the geometry of oblique incidence, which is required for the CPGE in (001)-oriented structures, additional pathways with intermediate states in the excited subbands $e2$, $e3$, etc also contribute to the radiation absorption. Such virtual transitions (path II) via states in the subband $e2$ are sketched in figures 5(d) and (e). The matrix elements of the transitions with intermediate states in the subband n ($n \neq 1$) have the form [8]

$$M^{(n)}_{\mathbf{k}'\mathbf{k}} = \mathrm{i}\frac{eA}{c\hbar}\left(\frac{\varepsilon_{n1}}{\varepsilon_{n1} - \hbar\omega} - \frac{\varepsilon_{n1}}{\varepsilon_{n1} + \hbar\omega}\right) e_z z_{n1} V_{1n}, \tag{7}$$

where ε_{n1} is the energy separation between the subbands at $\boldsymbol{k} = 0$, $z_{n1} = \int_{-\infty}^{+\infty} \phi_n(z) z \phi_1(z)\, dz$ is the coordinate matrix element, $\phi_n(z)$ is the function of size quantization, and V_{1n} is the matrix element of intersubband scattering. Equation (7) shows that this type of indirect transitions is independent of $\boldsymbol{k}$ and, consequently, also does not result in an electric current.

The photocurrent emerges due to quantum interference of the virtual transitions considered above. Indeed, the total probability for the real optical transition $\boldsymbol{k} \to \boldsymbol{k}'$ is given by the squared modulus of the sum of matrix elements describing individual pathways,

$$W_{\boldsymbol{k}'\boldsymbol{k}} \propto |M^{(1)}_{\boldsymbol{k}'\boldsymbol{k}} + \sum_{n\neq 1} M^{(n)}_{\boldsymbol{k}'\boldsymbol{k}}|^2 = |M^{(1)}_{\boldsymbol{k}'\boldsymbol{k}}|^2 + \left|\sum_{n\neq 1} M^{(n)}_{\boldsymbol{k}'\boldsymbol{k}}\right|^2 + 2\sum_{n\neq 1} \mathrm{Re}[M^{(1)}_{\boldsymbol{k}'\boldsymbol{k}} M^{(n)*}_{\boldsymbol{k}'\boldsymbol{k}}]. \tag{8}$$

Beside the probabilities of individual processes, it contains interference terms. By using equations (6) and (7) we derive

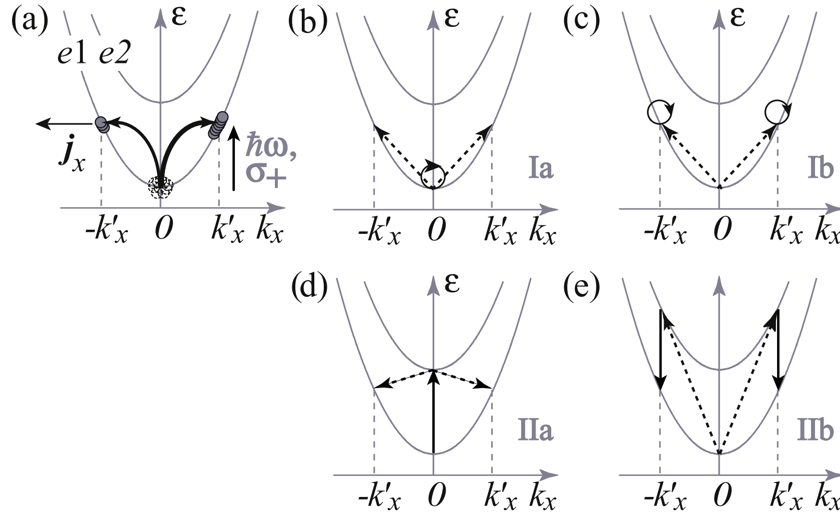

Figure 5. Microscopic model of the CPGE. Panel (a): indirect optical transitions due to free-carrier absorption of circularly polarized radiation are shown by bent arrows of various thicknesses indicating the difference in transition rates, which is caused by the quantum interference of various absorption pathways. Full circles sketch the resulting imbalance of the carrier distribution in $\boldsymbol{k}$-space yielding an electric current j_x. Panels (b)–(e): various pathways of the radiation absorption involving intermediate states in the subbands $e1$ and $e2$. Here, solid arrows indicate electron–photon interaction and the dashed arrows describe scattering events.

for the last terms on the right-hand side of equation (8)

$$\mathrm{Re}[M^{(1)}_{\boldsymbol{k}'\boldsymbol{k}}M^{(n)*}_{\boldsymbol{k}'\boldsymbol{k}}] = \mathrm{i}\frac{e^2A^2}{c^2m_\perp}\frac{\varepsilon_{n1}z_{n1}}{\varepsilon_{n1}^2-(\hbar\omega)^2}V_{11}V_{1n} \times[(k'_x-k_x)(e_ze_x^*-e_xe_z^*)+(k'_y-k_y)(e_ze_y^*-e_ye_z^*)]. \quad (9)$$

These terms are odd in the wavevector and, therefore, result in different rates for the transitions to $\boldsymbol{k}'$ and $-\boldsymbol{k}'$. This leads to an imbalance in the carrier distribution between $\boldsymbol{k}'$ and $-\boldsymbol{k}'$, i.e., to an electric current $\boldsymbol{j}$. Such a difference in real optical transition rates caused by constructive or destructive interference of various pathways is illustrated in figure 5(a). Moreover, it follows from equation (9) that the sign of the interference terms is determined by components of the vector product $\mathrm{i}[\boldsymbol{e}\times\boldsymbol{e}^*]$ and, therefore, by the radiation helicity because $\mathrm{i}[\boldsymbol{e}\times\boldsymbol{e}^*]=\hat{\boldsymbol{e}}P_{\mathrm{circ}}$. Thus, the imbalance of the carrier distribution in $\boldsymbol{k}$-space and, consequently, the photocurrent reverse upon switching the light helicity.

To calculate the photocurrent we assume that electrons populate only the ground subband, they are elastically scattered by short-range defects, and $\hbar\omega<\varepsilon_{21}$. Then, making an allowance for transitions via all electron subbands, one can write for the photocurrent [7, 8]

$$\boldsymbol{j} = e\frac{8\pi}{\hbar}\sum_{\boldsymbol{k},\boldsymbol{k}'}[\tau_{\mathrm{p}}(\varepsilon_{\boldsymbol{k}'})\boldsymbol{v}_{\boldsymbol{k}'}-\tau_{\mathrm{p}}(\varepsilon_{\boldsymbol{k}})\boldsymbol{v}_{\boldsymbol{k}}][f(\varepsilon_{\boldsymbol{k}})-f(\varepsilon_{\boldsymbol{k}'})] \times\sum_{n\neq1}2\,\mathrm{Re}[M^{(1)}_{\boldsymbol{k}'\boldsymbol{k}}M^{(n)*}_{\boldsymbol{k}'\boldsymbol{k}}]\delta(\varepsilon_{\boldsymbol{k}'}-\varepsilon_{\boldsymbol{k}}-\hbar\omega), \quad (10)$$

where τ_{p} is the momentum relaxation time, $\boldsymbol{v}_{\boldsymbol{k}}=\hbar\boldsymbol{k}/m_\perp$ is the electron velocity in the channel plane, $\varepsilon_{\boldsymbol{k}}=\hbar^2\boldsymbol{k}^2/(2m_\perp)$ is the electron kinetic energy measured from the subband bottom, $f(\varepsilon_{\boldsymbol{k}})$ the function of equilibrium carrier distribution in the subband $e1$, and the factor 8 in equation (10) accounts for the spin and valley degeneracy. For the electron scattering by short-range defects within the subband $e1$, the momentum relaxation time is given by $1/\tau_{\mathrm{p}} = m_\perp\langle V_{11}^2\rangle/\hbar^3$, where the angular brackets denote averaging over the impurity distribution.

Finally, summing up equation (10) over the wavevectors $\boldsymbol{k}$ and $\boldsymbol{k}'$ we derive the following expressions for components of the helicity dependent photocurrent:

$$j_x/I = e\frac{4\pi\alpha}{\omega n_\omega}\frac{\kappa\hbar}{m_\perp}\sum_{n\neq1}\frac{\langle V_{11}V_{1n}\rangle}{\langle V_{11}^2\rangle}\frac{\varepsilon_{n1}z_{n1}}{\varepsilon_{n1}^2-(\hbar\omega)^2}N_{\mathrm{s}}\hat{e}_yP_{\mathrm{circ}} \quad (11)$$

and $j_y=-(\hat{e}_x/\hat{e}_y)j_x$, where $\alpha=e^2/(\hbar c)$ is the fine-structure constant and κ is the dimensional parameter, which is given by

$$\kappa = \int_0^\infty(1+2\varepsilon/\hbar\omega)[f(\varepsilon)-f(\varepsilon+\hbar\omega)]\mathrm{d}\varepsilon\Big/\int_0^\infty f(\varepsilon)\,\mathrm{d}\varepsilon$$

and equal to 1 and 2 for the cases of $\hbar\omega\gg\bar{\varepsilon}$ and $\hbar\omega\ll\bar{\varepsilon}$, respectively, with $\bar{\varepsilon}$ being the mean kinetic energy of carriers in the equilibrium.

5.2. The CPGE in MOSFETs on miscut surfaces

In Si-MOSFETs fabricated on a miscut surface, the CPGE becomes possible even at normal incidence of radiation. This stems from the anisotropy of the electron dispersion in a valley together with the asymmetry of the confinement potential [6, 10]. The Hamiltonian describing electron states in the channel on a miscut surface in each of the low-energy valleys has the form (see, e.g. [7])

$$H = \frac{p_{x'}^2}{2m_{x'x'}}+\frac{p_{y'}^2}{2m_{y'y'}}+\frac{p_{z'}^2}{2m_{z'z'}}+\frac{p_{y'}p_{z'}}{m_{y'z'}}+V(z'), \quad (12)$$

where $\boldsymbol{p}$ is the momentum operator, $1/m_{\alpha\beta}$ is the tensor of the reciprocal effective masses with the non-zero components $m_{x'x'}=m_\perp$, $1/m_{y'y'}=\cos^2\vartheta/m_\perp+\sin^2\vartheta/m_\parallel$, $1/m_{z'z'}=\cos^2\vartheta/m_\parallel+\sin^2\vartheta/m_\perp$, $1/m_{y'z'}=(1/m_\perp-$

$1/m_\parallel)\cos\vartheta\sin\vartheta$, and $V(z')$ is the confining potential. The only non-trivial symmetry element, which does not change the Hamiltonian in equation (12) provided that $V(-z') \neq V(z')$, is the mirror reflection $x' \to -x'$. Thus, the Hamiltonian corresponds to the C_s point-group symmetry that allows the photocurrent in the geometry of normal incidence of radiation.

The eigen wavefunctions $\psi_{n\boldsymbol{k}}(\boldsymbol{\rho}', z')$ and energies $E_{n\boldsymbol{k}}$ of the Hamiltonian (12) are given by

$$\psi_{n\boldsymbol{k}}(\boldsymbol{\rho}', z') = \exp\left(\mathrm{i}\boldsymbol{k}\cdot\boldsymbol{\rho}' - i\frac{m_{z'z'}}{m_{y'z'}}k_{y'}z'\right)\phi_n(z'), \quad (13)$$

$$E_{n\boldsymbol{k}} = E_n + \frac{\hbar^2 k_{x'}^2}{2m_{x'x'}} + \frac{\hbar^2 k_{y'}^2}{2\tilde{m}_{y'y'}}, \quad (14)$$

where $\boldsymbol{\rho}' = (x', y')$ is the in-plane coordinate, $\phi_n(z')$ is the function of size quantization at $\boldsymbol{k} = 0$, E_n is the energy of the bottom of the subband n, and $1/\tilde{m}_{y'y'} = 1/m_{y'y'} - m_{z'z'}/m_{y'z'}^2$.

Similarly to the CPGE in (001)-oriented structures, the microscopic origin of the helicity dependent photocurrent in miscut structures is the quantum interference of virtual optical transitions with intermediate states in the ground and excited subbands. The latter processes are possible in structures on miscut surfaces even at normal incidence of radiation due to the presence of the off-diagonal component $p_{y'}p_{z'}/m_{y'z'}$ in the Hamiltonian, which couples the motion of carriers along the y' and z' axes. The matrix elements of virtual transitions via states in the ground and excited electron subbands have the form [10]

$$M_{\boldsymbol{k}'\boldsymbol{k}}^{(1)} = \frac{eA}{c\omega}\left[\frac{(k'_{x'} - k_{x'})e_{x'}}{m_{x'x'}} + \frac{(k'_{y'} - k_{y'})e_{y'}}{\tilde{m}_{y'y'}}\right]V_{11},$$
$$M_{\boldsymbol{k}'\boldsymbol{k}}^{(n)} = 2\mathrm{i}\frac{eA}{c\hbar}\frac{m_{z'z'}}{m_{y'z'}}\frac{\hbar\omega\varepsilon_{n1}z'_{n1}}{(\hbar\omega)^2 - \varepsilon_{n1}^2}e_{y'}V_{1n}. \quad (15)$$

Finally, calculating equation (10) with the matrix elements of equation (15) and taking into account that $1/\tau_p = \sqrt{m_{x'x'}\tilde{m}_{y'y'}}\langle V_{11}^2\rangle/\hbar^3$ in the case of short-range scattering, we derive

$$j_{x'}/I = e\frac{4\pi\alpha}{\omega n_\omega}\frac{\kappa\hbar}{m_{y'z'}}\frac{m_{z'z'}}{m_{x'x'}}\sqrt{\frac{\tilde{m}_{y'y'}}{m_{x'x'}}} \times \sum_{n\neq 1}\frac{\langle V_{11}V_{1n}\rangle}{\langle V_{11}^2\rangle}\frac{\varepsilon_{n1}z'_{n1}}{\varepsilon_{n1}^2 - (\hbar\omega)^2}N_s\hat{e}_{z'}P_{\mathrm{circ}}. \quad (16)$$

According to the symmetry analysis, the helicity dependent photocurrent induced by normally incident radiation arises to the extent of the channel plane deviation from the plane (001) together with the channel asymmetry. This follows also from equation (16), which demonstrates that the current $j_{y'}$ vanishes if the channel plane is parallel to (001), where $1/m_{y'z'} = 0$, or for the symmetrical structure, where $z'_{n1}\langle V_{11}V_{1n}\rangle = 0$ for any n.

6. Discussion

Equations (11) and (16) describe the main features of the circular photocurrent observed in electron channels on (001)-oriented and miscut silicon surfaces. In fact, it follows from equation (11) that the CPGE in (001)-oriented structures can occur only at oblique incidence and in the direction normal to the incidence plane. By contrast, in miscut structures, the circular photocurrent along x' can be excited even at normal incidence (see equation (16)). Such a behaviour of the CPGE in respect to the light propagation direction and crystallographic orientation has indeed been observed in all samples under study.

The microscopic origin of the circular photocurrent reversal upon variation of the energy separation between the subbands from $\varepsilon_{21} < \hbar\omega$ to $\varepsilon_{21} > \hbar\omega$ can be also clarified from equations (11) and (16). In the vicinity of the intersubband resonance, the spectral dependence of the photocurrent is given by $1/[\varepsilon_{n1}^2 - (\hbar\omega)^2]$, which stems from the matrix elements describing virtual transitions via the excited subbands, see equations (7) and (15). Thus, the photocurrent should increase drastically and undergo spectral inversion at $\hbar\omega \approx \varepsilon_{n1}$. In experiment, the resonant condition is obtained by tuning the intersubband separation with the gate voltage while the photon energy $\hbar\omega$ is fixed. Since at low temperatures only the ground subband is populated, the photocurrent inversion upon variation of V_g is observed for $\hbar\omega \approx \varepsilon_{21}$, see figure 3. While equations (11) and (16) yield sharp spectral resonances, in real structures the dependence smooths because of the broadening, but the inversion remains.

The magnitude of the CPGE detected in the transistor on the miscut surface with $\vartheta = 9.7°$ for $\hbar\omega = 8.4$ meV and $V_g = 3$ V is $J_x/P \sim 1$ nA W^{-1}, yielding the current density $j_x/I \sim 0.1$ nA cm W^{-1}. The same order of magnitude is obtained from equation (16) for the structure with the miscut angle $\vartheta = 9.7°$, the carrier density $N_s = 5 \times 10^{11}$ cm^{-2} ($V_g = 3$ V), the channel width $a = 8$ nm and the structure asymmetry degree $\langle V_{11}V_{12}\rangle/\langle V_{11}^2\rangle = 10^{-2}$.

In deriving equations (11) and (16) we considered the intrasubband optical transitions within the ground subband assuming that the momentum relaxation time τ_p is independent of the electron energy. Such an approximation is reasonable when the kinetic energy of photoexcited carriers is smaller than ε_{21}. For electrons generated with the energy $\varepsilon_{\boldsymbol{k}} > \varepsilon_{21}$ the momentum relaxation time gets shorter due to the additional relaxation channel caused by intersubband scattering. Consequently, one can expect that the magnitude of the CPGE current is smaller at $\hbar\omega > \varepsilon_{21}$ (low V_g) than that at $\hbar\omega < \varepsilon_{21}$ (high V_g). This can be responsible for the observed asymmetry in the gate voltage dependence of the photocurrent in the vicinity of the intersubband resonance, see figure 3. The gate voltage changes also the channel profile, which can be taken into account assuming that the ratios $\langle V_{11}V_{1n}\rangle/\langle V_{11}^2\rangle$ and the coordinate matrix elements z_{n1} depend on V_g. At $\hbar\omega \geqslant \varepsilon_{21}$, possible contributions to the CPGE due to intersubband optical transitions as well as scattering-induced broadening of the absorption peak should also be considered [6].

With increasing temperature the intersubband resonances are broadened and the excited subbands $e2$, $e3$, etc also become occupied at the equilibrium. This opens additional channels of the current formation including those with initial states in the excited subbands. As a result, both resonant LPGE and CPGE at $\hbar\omega \approx \varepsilon_{21}$ drastically decrease with

temperature (see figure 4), and the spectral behaviour of the photocurrent becomes more complicated. We observe that at room temperature the CPGE current inversion with the gate voltage is detected only for the photon energy $\hbar\omega = 16.3$ meV. Moreover, even in this case, the point of inversion does not correspond to $\hbar\omega = \varepsilon_{21}$.

7. Summary

In conclusion, we have studied the circular and linear photogalvanic effects in Si-MOSFETs under excitation with linearly and elliptically polarized radiation in the terahertz frequency range. The behaviour of photogalvanic effects upon variation of the radiation polarization state, wavelength, temperature, and bias voltage have been investigated in transistors prepared on (001) precisely oriented as well as miscut surfaces. The observed polarization dependence of the photocurrent is well described by the phenomenological theory of the photogalvanic effects based on symmetry analysis of the studied structures. Our experiments reveal that photon-helicity dependent currents of pure orbital origin can be generated in low-dimensional semiconductors even with the simple band structure and negligible spin–orbit interaction. The mechanism of photocurrent formation is based on the quantum interference of different pathways contributing to the radiation absorption. The microscopic theory of the circular photogalvanic effect under intrasubband (Drude-like) absorption in the ground electron subband has been developed and is in a good agreement with the experimental findings.

Acknowledgments

We thank E L Ivchenko, V V Bel'kov and J Kamann for helpful discussions. The financial support from the DFG, the Linkage Grant of IB of BMBF at DLR, Russian Ministry of Education and Sciences, and the RFBF is gratefully acknowledged. SAT acknowledges also the support from the Russian President Grant for young scientists (MD-1717.2009.2) and Foundation 'Dynasty'-ICFPM.

References

[1] Sturman B I and Fridkin V M 1992 *The Photovoltaic and Photorefractive Effects in Non-Centrosymmetric Materials* (Moscow: Nauka) (New York: Gordon and Breach)
[2] Ivchenko E L 2005 *Optical Spectroscopy of Semiconductor Nanostructures* (Harrow: Alpha Science Int.)
[3] Ganichev S D and Prettl W 2006 *Intense Terahertz Excitation of Semiconductors* (Oxford: Oxford University Press)
[4] Ivchenko E L and Ganichev S D 2008 *Spin Photogalvanics* (*Spin Physics in Semiconductors*) ed M I Dyakonov (Berlin: Springer) p 245
[5] Danilov S N, Wittmann B, Olbrich P, Eder W, Prettl W, Golub L E, Beregulin E V, Kvon Z D, Mikhailov N N, Dvoretsky S A, Shalygin V A, Vinh N Q, van der Meer A F G, Murdin B and Ganichev S D 2009 *J. Appl. Phys.* **105** 013106
[6] Magarill L I and Entin M V 1989 *Sov. Phys. Solid State* **31** 1299
[7] Ivchenko E L and Pikus G E 1997 *Superlattices and Other Heterostructures* (Berlin: Springer)
[8] Tarasenko S A 2007 *JETP Lett.* **85** 182
[9] Gusev G M, Kvon Z D, Magarill L I, Palkin A M, Sozinov V I, Shegai O A and Entin M V 1987 *JETP Lett.* **46** 33
[10] Olbrich P, Tarasenko S A, Reitmaier C, Karch J, Plohmann D, Kvon Z D and Ganichev S D 2009 *Phys. Rev.* B **79** 121302
[11] Knap W, Dyakonov M, Coquillat D, Teppe F, Dyakonova N, Lusakowski J, Karpierz K, Sakowicz M, Valusis G, Seliuta D, Kasalynas I, El Fatimy A, Meziani Y M and Otsuji T 2009 *J. Infrared Milli. Terahz. Waves* **30** 1319
[12] Ganichev S D, Ivchenko E L, Danilov S N, Eroms J, Wegscheider W, Weiss D and Prettl W 2001 *Phys. Rev. Lett.* **86** 4358
[13] Ganichev S D, Bel'kov V V, Schneider P, Ivchenko E L, Tarasenko S A, Wegscheider W, Weiss D, Schuh D, Beregulin E V and Prettl W 2003 *Phys. Rev.* B **68** 035319
[14] Ganichev S D and Prettl W 2003 *J. Phys.: Condens. Matter* **15** R935
[15] Bieler M, Laman N, van Driel H M and Smirl A L 2005 *Appl. Phys. Lett.* **86** 061102
[16] Reimann P 2002 *Phys. Rep.* **361** 57
[17] Ando T 1977 *Z. Phys.* B **26** 263
[18] Kneschaurek P, Kamgar A and Koch J F 1976 *Phys. Rev.* B **14** 1610
[19] Ando T, Fowler A B and Stern F 1982 *Rev. Mod. Phys.* **54** 437